EFFECT OF ARTIFICIAL AND NATURAL CRACKS ON WATER FLOW IN CONCRETE

Gang Li[1], Moh Boulfiza[2], Bing Si[3]

[1] Research Engineer, University of Saskatchewan, gang.li@usask.ca
[2] Associate professor, University of Saskatchewan, moh.boulfiza@usask.ca
[3] Professor, University of Saskatchewan, bing.si@usask.ca

ABSTRACT

Cracks dramatically increase the permeability of concrete. In reinforced concrete structures, cracks provide pathways for water and adverse ion species to reach the embedded rebar causing premature deterioration. The objective of this study is to investigate how cracks affect the water flow in concrete. Experimental tests were carried out on cracked reinforced concrete specimens exposed to wetting and drying scenarios. Two types of cracks were investigated: parallel-wall artificial cracks and flexural loading induced natural cracks. Each type has two levels of crack width, 0.3 mm and 1.0 mm. The evolution of water content around the cracks was monitored by the Time Domain Reflectometry (TDR) technique. It was found that both types of cracks behaved like an open surface that is exposed to the environment.

Keywords: Crack, Concrete, Water content, Saturation, TDR

Gang Li, MSc, EIT
University of Saskatchewan
57 Campus Drive
Saskatoon, SK S7N 5A9
Canada

Email: gang.li@usask.ca
Tel: 306-966-5377

1. INTRODUCTION

Reinforced concrete is known for its great structural performance and durability. The rebar strengthens the concrete in tension and the concrete protects the rebar from corroding. In most cases, reinforced concrete structures would be in good condition within their service life. However, the presence of cracks provides pathways to water flow, and the water flow further carries aggressive agents such as chloride ions, which facilitate the corrosion of the rebar and adversely affects the durability of reinforced concrete structures. Therefore it is significant to understand how cracks would affect the water flow in concrete especially in the cracking area.

Despite the fact that water flow in cracked concrete play a major role in the long-term performance of reinforced concrete, only a limited amount of research has been reported on effect of cracks on water flow in concrete. More studies focus on the effect of cracks on chloride content profile distribution around the crack after certain period of salt solution exposure [1,2,3,4,5]. These studies did not treat the water flow as a contributing factor of chloride diffusion. The exposure condition employed, such as ponding and diffusion cell, did not include wetting and drying cycles thus no water fluctuation. When wetting and drying exposure conditions were considered, e.g. [6], there were no reported results on the saturation change during the exposure period. However, wetting and drying conditions are very common for field structures such as bridge deck, parking garage etc. Therefore, an understanding of water flow in cracked concrete under wetting and drying conditions would benefit the evaluation and prediction of the deterioration of reinforced concrete structures.

Although the permeability of cracked concrete with cracks was studied [3,7], some limitations still exist: the saturation condition in the vicinity of cracks was not studied. In addition, the crack pattern does not resemble the crack in the real case and it was also pointed out by the author [7] that the cracks generated by the splitting tests may be identical in widths through the crack walls. However, in the actual structures, the curvature of flexural members, or the gradient of stress distribution will result in narrower crack widths at the level of the steel than at the surface.

In this study, four types of cracked concrete beams were cast: two crack types, natural flexural cracks, and parallel-wall artificial cracks, two levels of crack openings, 0.3 mm and 1.0 mm, representative of ranges where the corrosion rate has been observed to be negligible and where it becomes significant respectively [8,9,10]. The apparent hydraulic conductivity of the cracked concrete samples was evaluated by a tension infiltration test. Time Domain Reflectometry (TDR) was adopted to measure the water saturation under wetting and drying conditions around artificial and natural cracks.

2. EXPERIMENTAL METHODS

2.1. Preparation of specimens

2.1.1. Materials

Ordinary Portland cement (CSA A5 Type GU) was used as the cementitious material for all samples in this project. The mix proportioning design was based on the ACI 211.1 manual with a fixed sand ratio of 35% (Table 1). The 28 days compressive strength of concrete was 33.5 MPa. A single No.10 Plain carbon steel rebar was placed in the flexural cracking specimens the maximum diameter of aggregate was 0.5 cm. Large gravels were not used in the concrete mixing because those gravels would interfere with probes, causing the stainless probes to bend. A superplasticizer was added to increase the workability so that the mixture was cohesive and self-compacting. A good workability helps to build sound bonding between concrete and probes.

Table 1. Concrete mix proportions

Mix proportions (kg/m^3)				w/c	f_c' at 28 days (MPa)
Cement	Water	Fine aggregate	Coarse aggregate		
448.9	202.0	542.2	855.9	0.45	33.5

Two types of beams were cast: short beams and long beams where artificial cracks and natural cracks were induced respectively. The beam configuration and size depicted in Figure 1. The samples were demoulded after 24 hours and cured in the curing room with a temperature 23± 2℃ for 28 days.

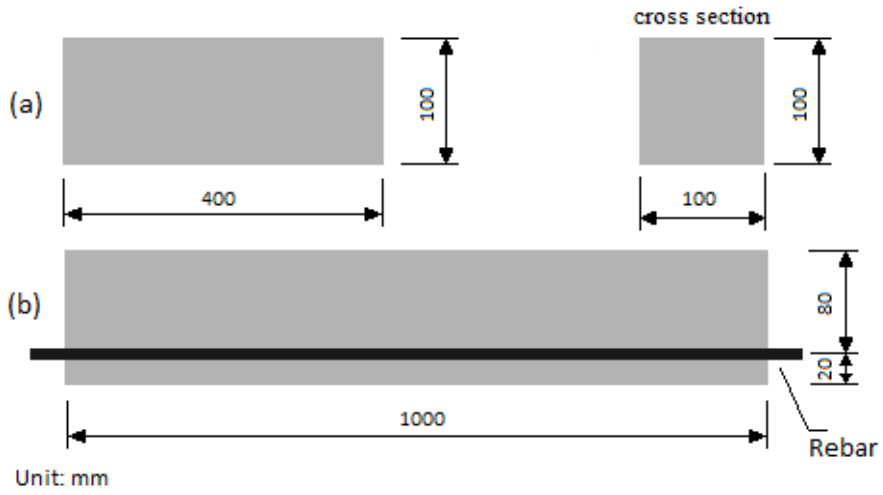

Figure 1. Beam sample configuration. (a) Short beam, (b) Long beam.

2.1.2. Creation of cracks

Artificial cracks

The artificial cracks were created by pulling out the pre-inserted shims. Shims with a 60×100 mm cross section and thicknesses of either 0.3 mm or 1.0 mm were glued to the side wall of the mould. During casting, the mixture was poured simultaneously from both sides of the shim to ensure an equal pressure was acting on both sides of the shim. 3 hours after casting, C-clamps were used to gently pull out 5 mm of the shim and then after 24 hours curing the shim was pulled out completely. Once the crack was shaped, samples were placed in the curing room for 28 days.

Natural cracks

The natural cracks were created by a three-point flexural loading. The long beam was positioned on the compression machine in a manner such that the single rebar was in the compression zone. The single crack could be generated when the notched mid-span concrete reached its fracture strength, and because the fracture was not reinforced by a rebar, it was convenient to keep it open at desired width by inserting shims.

The samples were subjected to a three-point loading test with a 0.9 m span. The test configuration setup is shown in Figure 2. The loading was conducted at a rate of 3 N/s and was programmed to stop when a sudden 10% percent drop of the crack took place. Cracks were generated at load values in the range of 1500-1800 N. Once a crack was created, it could be easily re-opened later by adjusting the fine-position knob. After the coating treatment was done (see Section 2.1.4), Shims with thicknesses of 0.3 mm and 1.0 mm were used to maintain the crack openings 0.3 mm and 1.0 mm wide.

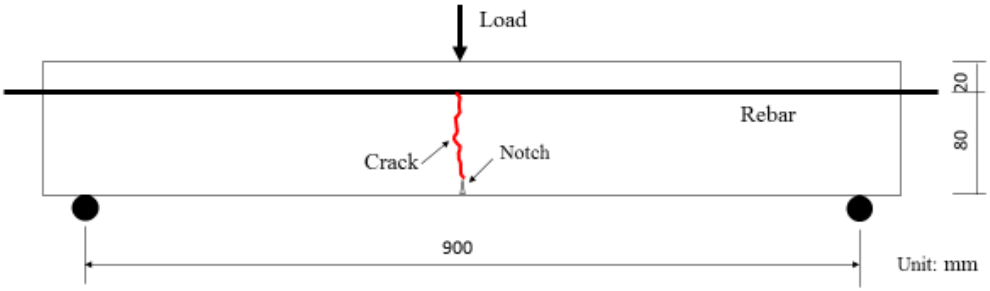

Figure 2. Three-point flexural loading test.

2.1.3. Probe installation

The TDR probes were installed in the beam around the crack obtain the profile of water content. The probes were inserted from the lateral surface of the sample (or the top finishing surface before demoulding; the samples were side-cast) through a probe holder (Figure 3a) when the concrete was in its plastic state. For the unreinforced short beam 9x8 probes were installed and for the reinforced long beam, probes on Row 7 were excluded to avoid the rebar at that position (Figure 3b). In each column the every two neighbouring probes acted as a two-rod probe when connected to the TDR cable tester.

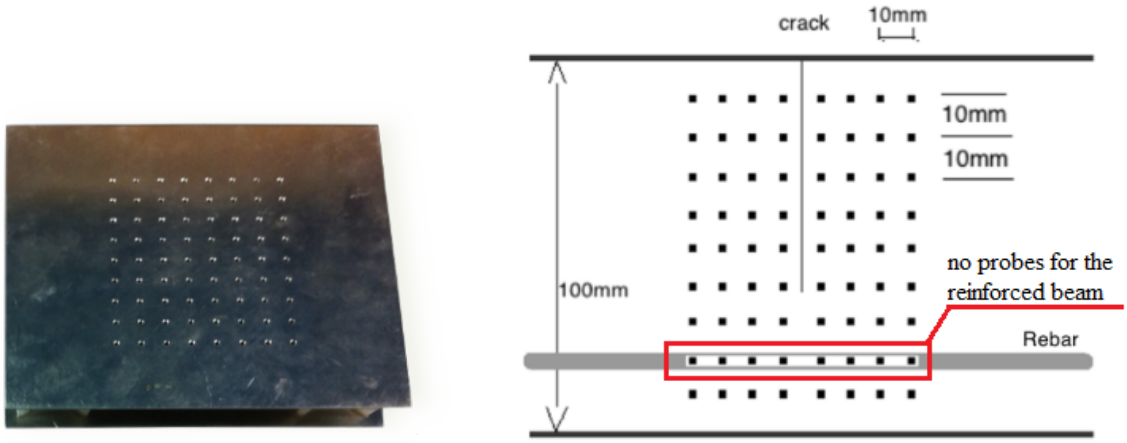

(a) (b)

Figure 3. (a) Double-layered probe holder, (b) Schematic of the probe map, the black dots indicate the location where the probes are inserted.

2.1.4. Coating

All sides of the samples were coated with epoxy, except the finish surface, which allowed one-dimensional transport of moisture and was more representative of many large field structures, such as bridge decks. All samples were cleaned by a compressed-air blower to remove any dust or debris. Three layers of coating were applied to the samples to ensure the fill of all open pores in the concrete surface. After each coating was applied, one-week curing time was allowed for the epoxy to cure.

2.2. Wetting and drying exposure

For the wetting session, the specimens were submerged in water with the uncoated surface facing up, about 5 cm under the water surface. For the drying session, the beams were exposed to the ambient air in the laboratory environment, which is 40±2% RH, and 23 ℃.

2.3. TDR probe calibration

Concrete is a multi-phase material that contains solid, gas, and liquid. Each phase has a different dielectric constant value and the dielectric constant of the mixture reflects the fraction of each phase by volume. Usually, the dielectric constant of water is taken as 80, and for air its value is 1. In concrete, other dry solid phases have a value between 2.2 and 5.4 (Table 2). Among all compositions, water has the largest dielectric constant, which means that the water content of concrete is highly sensitive to the dielectric constant.

Calibration of dielectric constant and water content was conducted by measuring the dielectric constant of concrete samples in different saturation levels. Six calibration samples (10 cm ×10 cm × 3±0.5 cm) with TDR probes pre-installed were sawed off from one short beam, which were made with the same concrete as that of the tested beams. These six samples were submerged for three months to reach fully saturation.

Table 2. Comparison of measured to known and calculated dielectric constant [11]

Material	Dielectric constant	
	Measured	Known/calculated
Sand, od*	2.9	3.02
Coarse aggregate, od	2.2	3.45
Unhydrated cement	2.7	2.83
Concrete, od	5.4	5.49
Mortar, od	3.9	4.99

*od: oven dried

The different levels of saturation were obtained by stepped oven drying the sample from full saturation. A total of eight times of drying steps were taken. Each time, the specimens were placed into a 105 ℃ drying oven for 2-3 hours; the final drying was conducted for 24 hours. After each drying step, the samples were removed from the oven, wrapped and sealed in plastic bags and kept for 3 days to allow the moisture to get evenly distributed in the specimens. For each water content level, the water content of the sample was measured by weight; the dielectric the TDR cable tester. The time allowed for the water to equalize is conservative; it was decided based on Korhonen's experiment [11], where a much larger cylinder specimen was used. Also the calibration data were read from different locations of the specimen, they did not show an uneven water distribution in the specimen.

2.4. Measuring the evolution of saturation

The TDR test setup consists of a cable tester (Tektronix 1502B), coaxial cable, and stainless probes embedded in concrete samples. The specimens were subjected to wetting and drying cycles. The dielectric constant was measured from the probes grids. As illustrated in Figure 3(b), each two vertical neighbouring probes formed a two-rod probe, or probe pair, which gave eight probe pair in each column (9 probes) for unreinforced samples and 6 probe pair in each column (7 probes) for reinforced samples. Both types of samples had eight columns of probe pair, which gave 8×8 data and 8×6 data for the artificial crack samples and the natural crack samples, respectively. During wetting cycle, the samples were taken out and measured by TDR system, at 0, 1, 3, 5, 8, 13, 22, 33, 56, 80, 128, 200, 296 hours. When the samples were taken out of the ponding solution, they were immediately wrapped with a plastic membrane to prevent evaporation from the surface. During the drying cycle, the dielectric constant was measured at 0, 4, 11, 23, 47, 95, 167, 263, 407, 695 hours.

3. RESULTS AND DISCUSSION

3.1. Water content and dielectric constant relation

For each calibration sample, seven readings were made from seven pairs of probes formed by eight probes in each sample. The water content θ and accordingly the dielectric constant κ of six samples were recorded during the stepped drying process.

Four possible equations, including polynomials from 1 to 4 degrees, have been studied for curve fitting; see fit 1 to fit 4 in Figure 4. The 3-degree and 4-degree polynomial might be best fit for the given data to have a maximum R^2 statistically. However, these two high degree polynomials are considered as over fitting, because the two curves become flat at both lower and higher end of κ, which does not agree with the trend of data that greater water content gives greater dielectric constant; for example at the lower end of the fit3 and fit4, the water content decreases with the increase of dielectric constant. Therefore, only 1-degree (linear) and 2-degree (quadratic) polynomials fitting models are considered and discussed below.

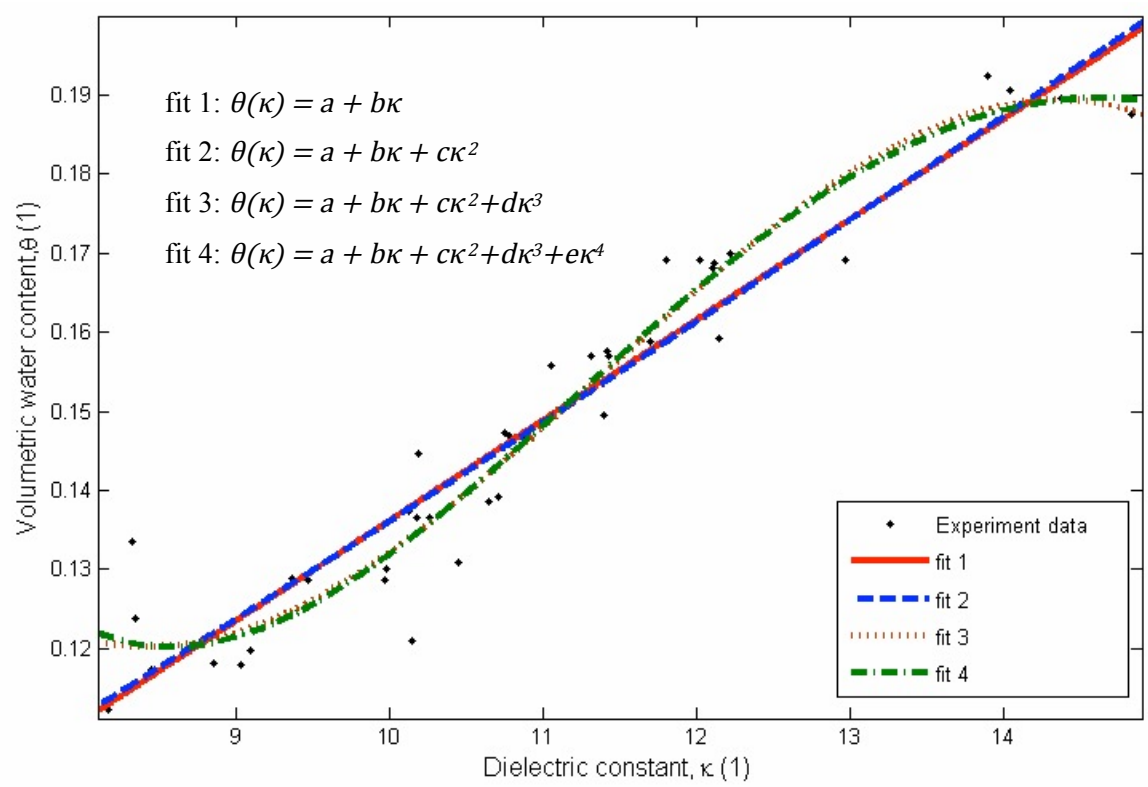

Figure 4. Water content- dielectric constant curve fitting options.

For the 2-degree (quadratic) polynomial model:

$$\theta(\kappa) = a + b\kappa + c\kappa^2 \quad (1)$$

where κ is the dielectric constant and θ is the volumetric water constant. As listed in Table 3, the p-value of the κ^2 coefficient is 0.7658. This is much greater than 0.05, which suggests that the estimated coefficient of κ^2 is not significant. Therefore, there is no need for a quadratic model and the linear model is sufficient.

$$\theta(\kappa) = a + b\kappa \quad (2)$$

Hence, the dependence of water content on dielectric constant is given by Eq. (3).

$$\theta = 0.012679\kappa + 0.00933 \quad (3)$$

Table 3. Statistics of 2-degree polynomial regression (fit 2)

Estimated Coefficients	Estimate	SE	tStat	pValue
Intercept	0.020154	0.036663	0.5497	0.58566
b	1.6482	0.010734	0.0065126	0.10735
c	8.531e-05	0.00028446	0.29991	0.76584

SE: standard error, tStat: t-statistic, Significance at pValue<0.05

The data points and linear model regression with 95% confidence bounds for the regression function are shown in Figure 5. The 95% prediction bounds suggests that there is a 95% chance that water content-dielectric constant relationship function will fall in the envelope formed by red-dotted lines, which gives a water content error no greater than ±0.005 or 0.5% by volume for a given dielectric constant.

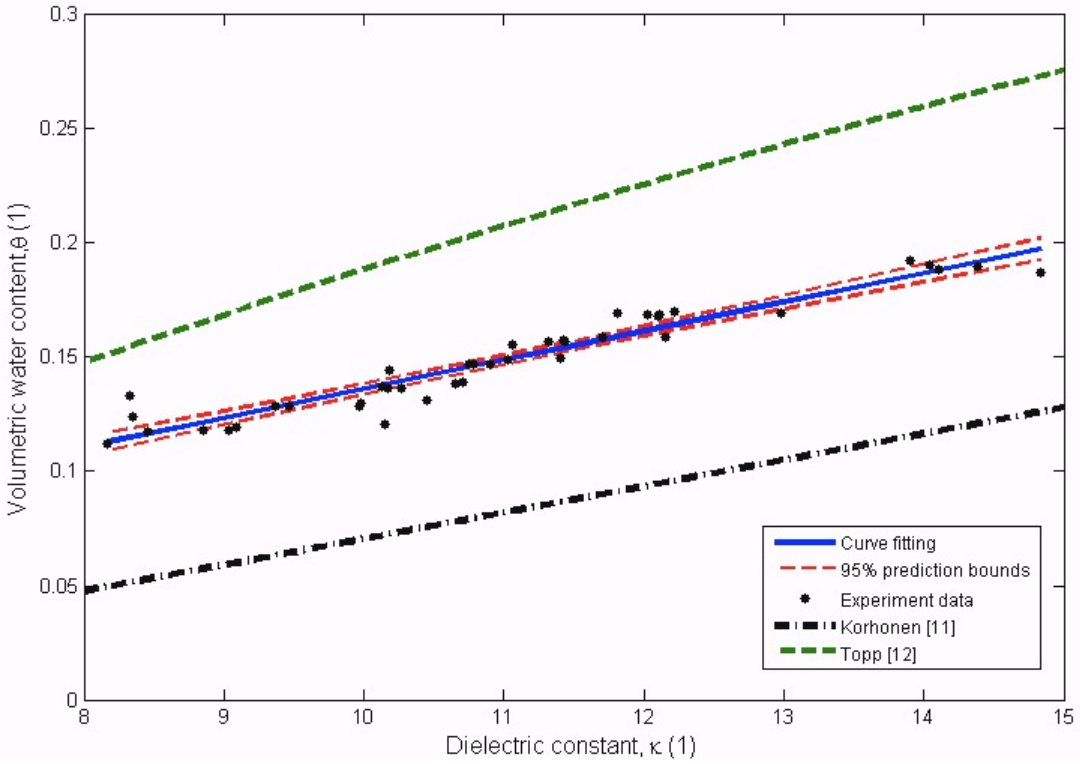

Figure 5. Volumetric water content-Dielectric constant relation.

The relationship between water content and dielectric constant is similar to the well-known Topp's Equation [12] for soils. However, an overall drop of the water content is observed for the concrete, for dielectric constant in the tested range. This means that for a similar dielectric constant, concrete has a lower water content than soil by approximately 0.06. Korhonen et al also observed a similar trend in the TDR calibration test with a drop of roughly 0.05 and 0.10 for concrete and mortar, respectively [11]. Hardened cement paste has a specific surface area that is several orders of magnitude greater than that of unhydrated cement, sand, coarse aggregate. Since bonded water has a lower dielectric constant than bulk water [13,14], a material with higher surface area and thus larger portion of bonded water would be expected to have a lower dielectric constant for the same water content. Comparing to Korhonen's experiment, the concrete used in this paper has finer aggregates, more like mortar, which gives the material larger specific area, more bonded water and thus higher water content at a given dielectric constant.

3.2. Saturation profile

The volumetric water content was tested with TDR following the steps described in Section 2.4. As shown in Figure 6, the round solid marks indicate the location where probes were inserted. Every two vertical neighboring probes were employed as a two-rod probe pair to send and receive signals by a Tektronix 1502B/C Cable Tester. The surrounding lines show the signal distribution and the x marks represent the location, for which the water content was recorded. It was assumed that the water content at locations marked as x location was equal to the averaged water content for the signal covered area. For the unreinforced beams, 8 (row number) ×8 (column number) datasets were collected and for the reinforced beams, 6×8 datasets were collected omitting the probe row at the rebar location and ignoring the last row of probes. The row of probes above and below the rebar could have been used by connecting horizontal rods in the same row. However, the signal distribution from those horizontal probes was too close to the rebar, and hence was affected by the presence of rebar causing a distortion of the waveform. Although using the non-conductive FRP-based rebar might have reduced the distortion, it brings effects on the TDR test as well for it has a very different permittivity than that of the surrounding concrete material. The significance of the effect on distortion of the waveform by other materials was not investigated in this study.

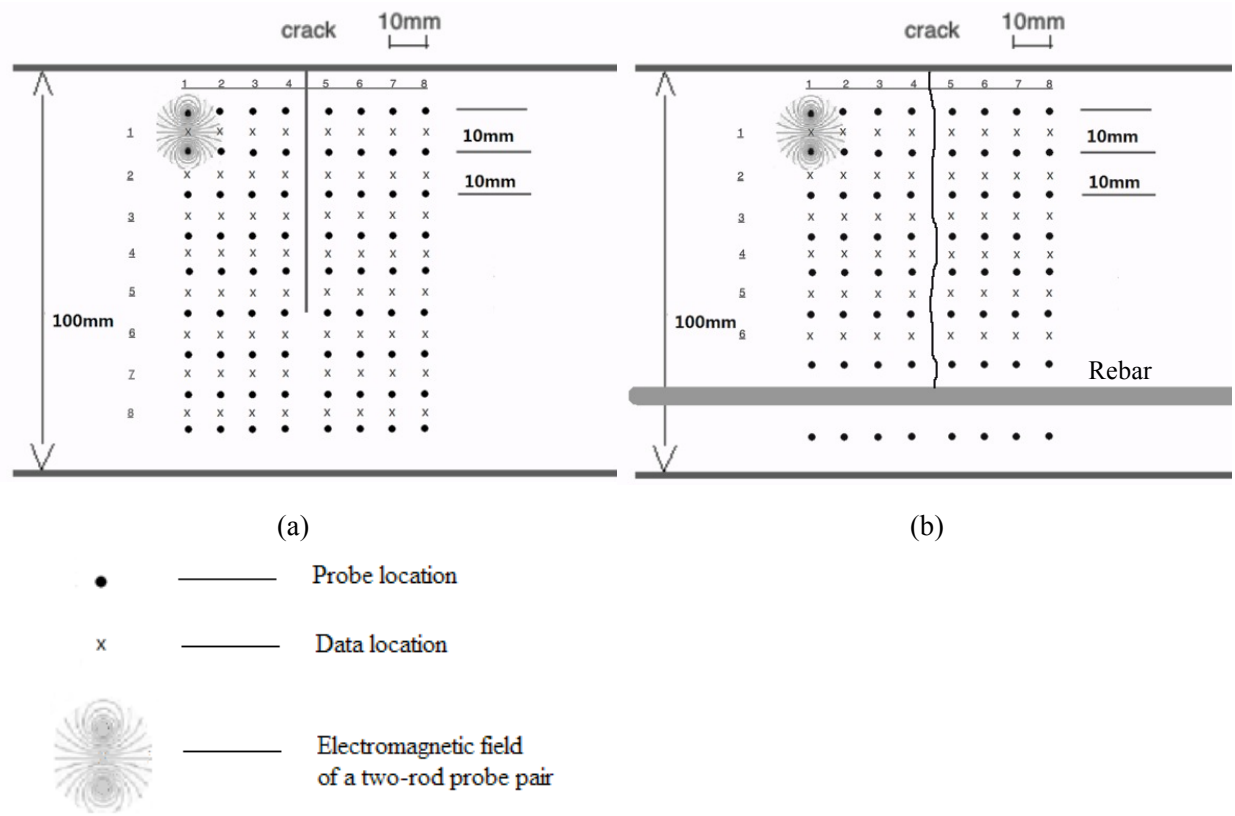

Figure 6. The location of data collection. (a) a schematic diagram of data grid on an artificial crack sample (b) a schematic diagram of data grid in on a natural crack sample.

The matrix of dielectric data were collected and then converted to volumetric water content through the calibration. The distribution of water content in the probed area was presented by colour-scaled images. Between the 8×8 or 6×8 data sets, a linear interpolation was employed to improve the data visualization.

3.2.1. Wetting cycle

Typical colour-scale plots are shown in Figure 7, for the saturation conditions at 5 hours of water ponding, for example. The artificial cracks are shown as a straight line at the middle position and the natural cracks are shown with two lines digitized from the real crack shape, a solid line for the front face, a dotted line for the back face, and a dash-dotted line representing the averaged crack shape of front and back cracks.

The initial saturation condition for the air-dried samples, at ambient conditions in the lab, ranged from 0.4 to 0.7. Drier areas were found near the crack. The water penetration proceeded at a fairly high rate: From air-dried state, 4 samples with different types of cracks reached full saturation at 296 hours (about 12 days). In the first hour, water saturation started quickly at the cracks' surface except for the natural crack with 0.3 mm opening, which may be caused by trapped air in the narrow crack. It can also be observed that, in a finer scale water penetrates through a "preferred path". For example, higher levels of saturation are seen at the locations (x, y)=(70,70), (35,70) in Figure 7(a), (b), which is different than the ideally distributed 2D water contour. This is probably due to the localized micro cracks generated during the shim pull-out when the artificial cracks were generated or due to a non-uniform compaction around the shim insertion. For samples with artificial cracks, the water penetration front agrees well with the crack geometry and sample symmetry as the water front profile is close to a 2D diffusion problem from both the top open surface and the crack surface. For samples with natural cracks, because of the 3D geometric crack and possible damage in the matrix near the crack, it is acting more like a "cracked zone" with a higher permeability, on average.

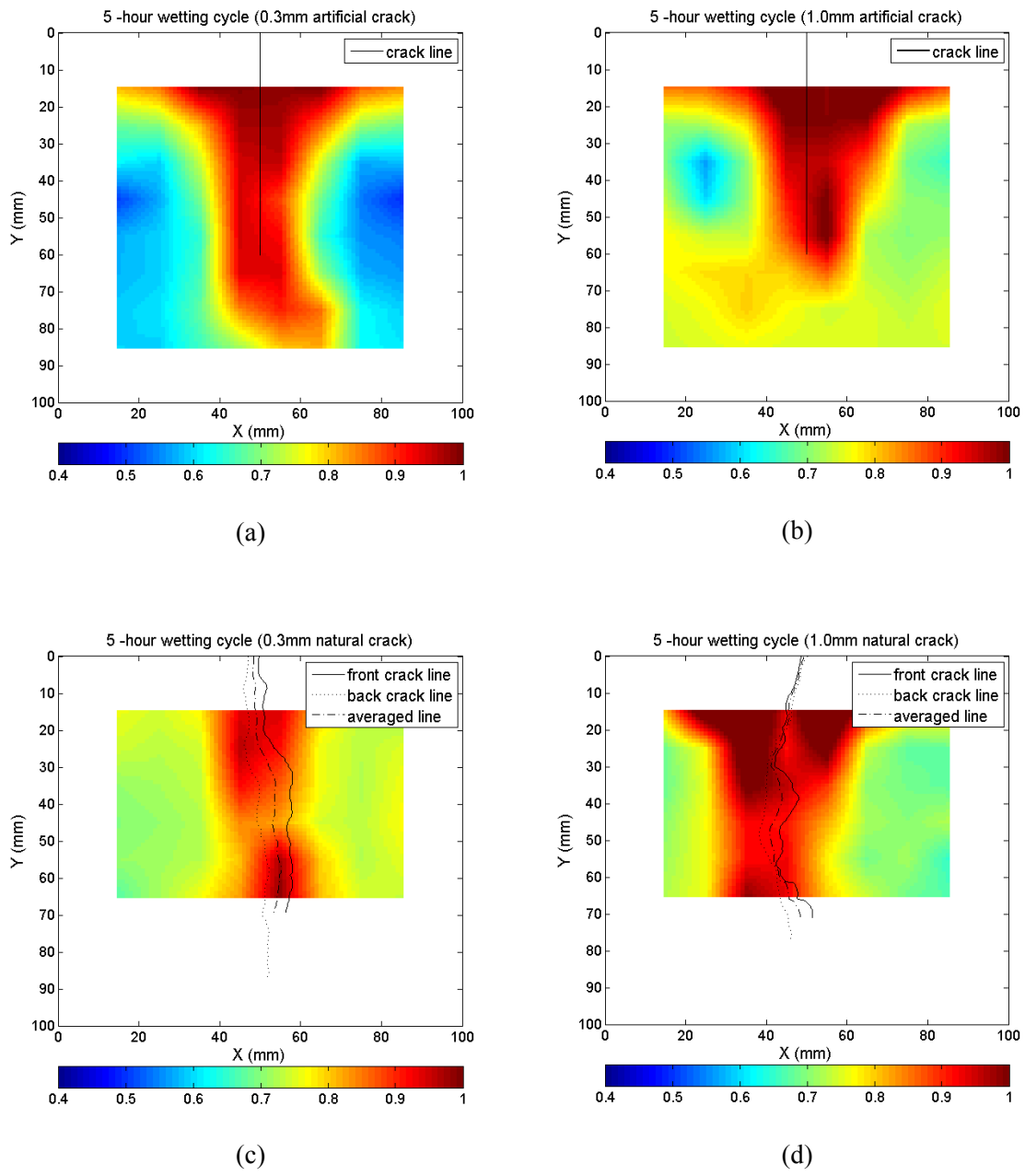

Figure 7. Typical colour-scaled images of the saturation conditions for concrete with 4 types of crack after 5-hour's wetting. (a) 0.3 mm artificial crack; (b) 1.0 mm artificial crack; (c) 0.3 mm natural crack; (d) 1.0 mm natural crack.

3.2.2. Drying cycle

The typical colour-scaled plots for the saturation conditions at 695 hours of exposure to ambient air at in a RH=40±2% room condition, are shown in Figure 8. The artificial cracks are shown as a straight line at the middle position and the natural cracks are shown with two lines digitized from the real crack shape, a solid line for the front face, a dotted line for the back face, and a dash-dotted line representing the averaged crack shape of front and back cracks.

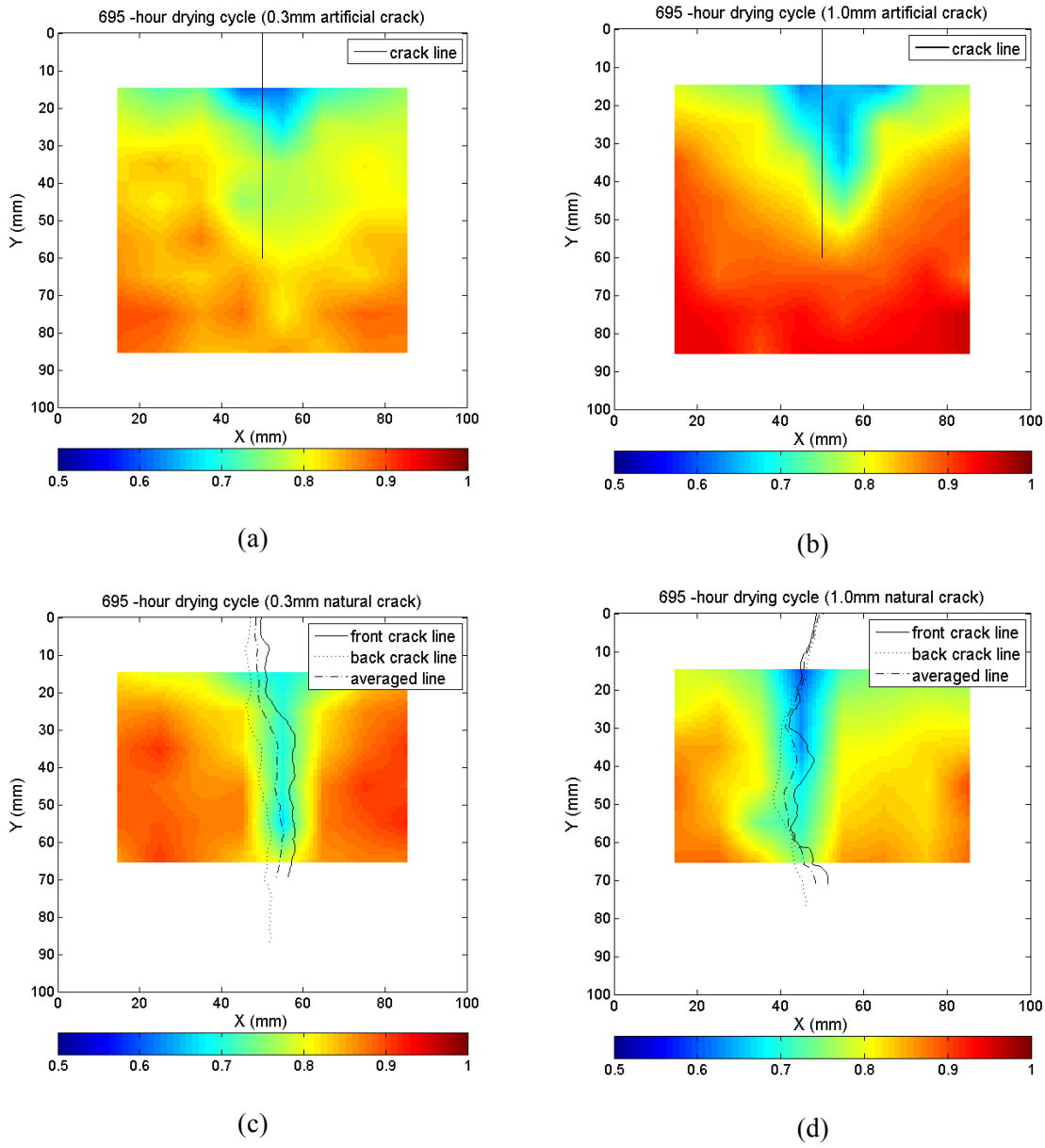

Figure 8. Typical colour-scaled images of the saturation conditions for concrete with 4 types of crack after 695-hour's drying. (a) 0.3 mm artificial crack; (b) 1.0 mm artificial crack; (c) 0.3 mm natural crack; (d) 1.0 mm natural crack.

The drying phase started from a fully saturated condition. In the drying phase, water was lost from the sample at a much lower rate than the infiltration of water in the wetting phase. It took 2855 hours (about four months) for the sample to reach a saturation state similar to the air-dried initial value in the wetting phase, while it only took less than two weeks for those air dried samples to reach full saturation. For both artificial crack samples and natural crack samples, water loss took place at a faster rate around the larger cracks. For the artificial ones, the "faster-dried region" did not have the same length as the length of the crack (60 mm) because of the water content values gained from TDR are averaged with the value of non-cracked part (60 mm deeper from the open surface); for natural ones, the driest regions were more closely confined around the cracking paths as the crack goes through the whole data mapping area.

3.2.3. Crack surface vs. free surface

In order to find out if the crack surface behaves like the upper free surface, the saturation change with time at a depth of 1.5 cm into concrete from both free surface and crack surface are plotted in Figure 9 for wetting cycle and Figure 10 for drying cycle. Data points near the free surface, with a horizontal distance of 3.5 cm and 2.5 cm from the crack line, are denoted as "exp-s3.5" and "exp-s2.5". Data points near the crack surface, with a vertical distance of 3.5 cm and 2.5 cm from the free surface, are denoted as "exp-c3.5" and "exp-c2.5"). The saturation values are averaged from the left and right sides of the crack.

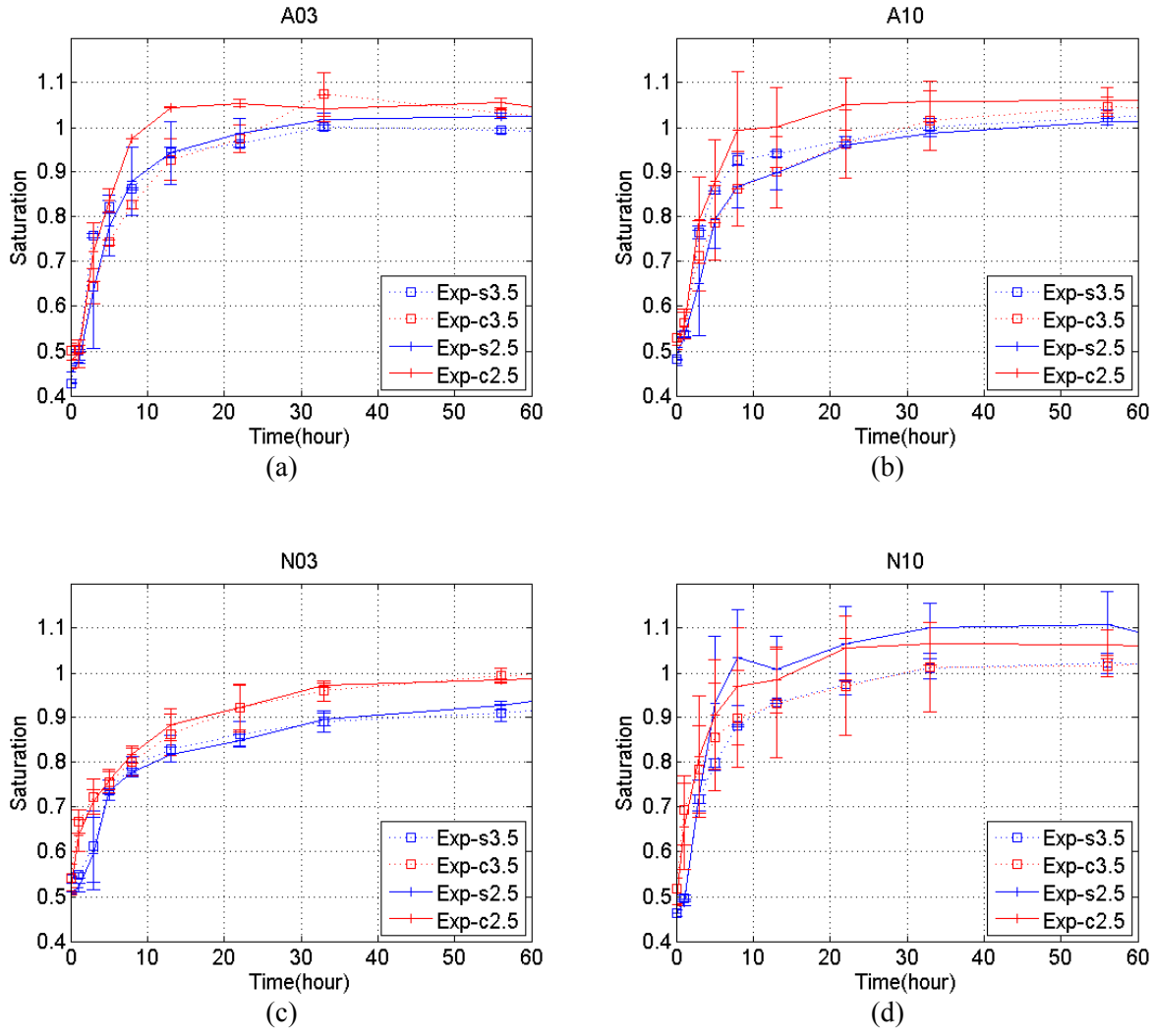

Figure 9. Saturation change vs. time for near-surface point (exp-s3.5/2.5) and near-crack point (exp-c3.5/2.5) in the wetting phase. (a) A03: Artificial crack with surface crack opening of 0.3 mm; (b) A10: Artificial crack with surface crack opening of 1.0 mm; (c) N03: Natural crack with surface crack opening of 0.3 mm; (d) N10: Natural crack with surface crack opening of 1.0 mm).

The results show that larger variations are found for the cracks with 1 mm surface openings in the first 40 hours. The saturation changes look very similar for both the near-surface point and the near-crack point, which suggests that water transport through open surface and through the crack surface have a similar behaviour. Also, for the drying phase, it can be seen from Figure 10 for all types of cracks. Drying rate at the near-surface point is slightly larger than that at the near-crack point. The maximum difference is 0.05 in saturation level. This shows that it would be reasonable to model the crack with the same behaviour as an open free surface without a very large error in water saturation levels.

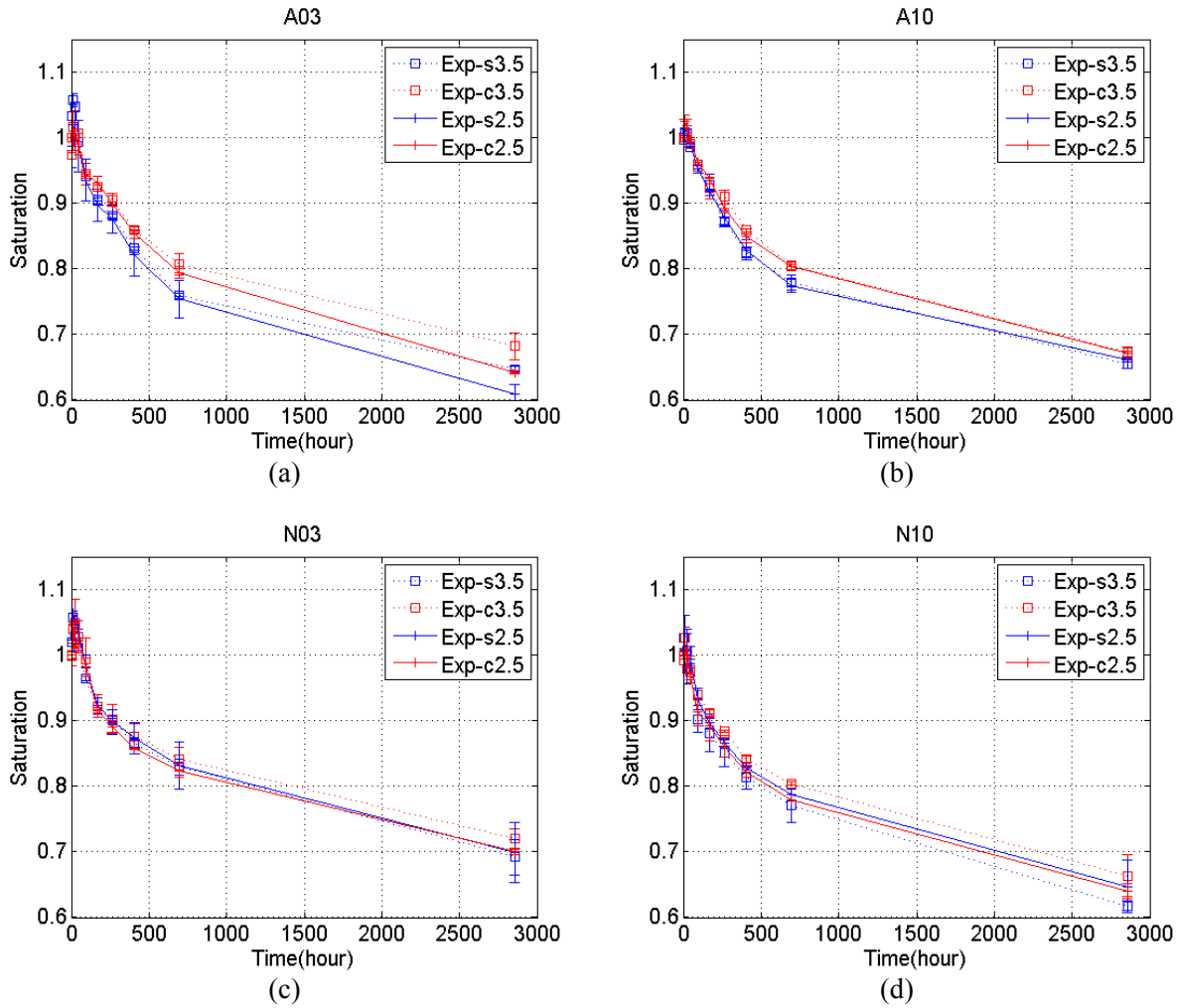

Figure 10. Saturation change vs. time for near surface point (exp-s3.5/2.5) and near crack point (exp-c3.5/2.5) in the drying phase. (a) A03: Artificial crack with surface crack opening of 0.3 mm; (b) A10: Artificial crack with surface crack opening of 1.0 mm; (c) N03: Natural crack with surface crack opening of 0.3 mm; (d) N10: Natural crack with surface crack opening of 1.0 mm).

4. CONCLUSIONS

A Time Domain Reflectometry (TDR) test was developed for monitoring the evolution of water saturation around the crack over time. A linear regression model was used to relate the volumetric water content and dielectric constant in concrete.

The evolution of water saturation of the cracked concrete under wetting and drying conditions was analyzed as colour-scaled images and the water saturation contours were compared for different crack openings. For the artificial cracks, the water saturation level was symmetrically distributed around the cracks, except for the deviated regime observed around the tip of a straight crack. This was probably caused by the damage in form of micro cracks induced during the shim pull-out process and due to a non-uniform compaction around the shim, the mico cracks are prone to develop towards one side of the crack, such that at the tip of a crack, water flows preferably to one side. For the natural cracks, in the drying phase, smaller cracks seemed to have better water storage. Hence, the water saturation decreased at a slightly slower rate as compared to larger natural cracks.

The crack surface of both crack types (artificial and natural) and sizes (0.3 mm and 1.0 mm) had a similar influence as the open surface on the water transport. The crack could be modelled as an open free surface without inducing a very large error in water saturation levels.

ACKNOWLEDGMENTS

The authors gratefully acknowledges for the financial support provided by the China Scholarship Council and the Department of Civil and Geological Engineering, University of Saskatchewan.

REFERENCES

[1] Rodriguez, O. G., & Hooton, R. D. (2003). Influence of cracks on chloride ingress into concrete. *ACI Materials Journal,* 100(2).

[2] Win, P. P., Watanabe, M., & Machida, A. (2004). Penetration profile of chloride ion in cracked reinforced concrete. *Cement and Concrete Research,* 34(7), 1073-1079.

[3] Aldea, C., Shah, S. P., & Karr, A. (1999). Effect of cracking on water and chloride permeability of concrete. *Journal of Materials in Civil Engineering, 11*(3), 181-187.

[4] Ismail, M., Toumi, A., Francois, R., & Gagné, R. (2004). Effect of crack opening on the local diffusion of chloride in inert materials. *Cement and Concrete Research, 34*(4), 711-716.

[5] Gowripalan, N., Sirivivatnanon, V., & Lim, C. (2000). Chloride diffusivity of concrete cracked in flexure. *Cement and Concrete Research, 30*(5), 725-730.

[6] Mohammed, T. U., Otsuki, N., Hisada, M., & Shibata, T. (2001). Effect of crack width and bar types on corrosion of steel in concrete. *Journal of Materials in Civil Engineering*, 13, 194.

[7] Wang, K., Jansen, D. C., Shah, S. P., & Karr, A. F. (1997). Permeability study of cracked concrete. *Cement and Concrete Research,* 27(3), 381-393.

[8] Pettersson, K. (1996). Criteria for cracks in connection with corrosion in high-strength concrete, 4th int. *Symp. Utilisation of High-Strength/High-Performance Concrete, Paris,* 509-517.

[9] Schiessl, P., & Raupach, M. (1997). Laboratory studies and calculations on the influence of crack width on chloride-induced corrosion of steel in concrete. *ACI Materials Journal*, 94(1).

[10] Jaffer, S. J., & Hansson, C. M. (2009). Chloride-induced corrosion products of steel in cracked-concrete subjected to different loading conditions. *Cement and Concrete Research, 39*(2), 116-125.

[11] Korhonen, C. J., Janoo, V. C., & Berini, C. M. (1997). *Time-Domain Reflectometry of Water Content in Portland Cement Concrete*, No. CRREL-SP-97-27). Cold regions research and engineering lab, Hanover, NH, USA.

[12] Topp, G., Davis, J., & Annan, A. P. (1980). Electromagnetic determination of soil water content: Measurements in coaxial transmission lines. *Water Resour.Res, 16*(3), 574-582.

[13] Jacobsen, O. H., & Schjønning, P. (1993). Field evaluation of time domain reflectometry for soil water measurements. *Journal of Hydrology,151*(2), 159-172.

[14] Jacobsen, O. H., & Schjønning, P. (1993). A laboratory calibration of time domain reflectometry for soil water measurement including effects of bulk density and texture. *Journal of Hydrology,151*(2), 147-157.